Morphology and Surface Area of Emulsion-Derived (PolyHIPE) Solid Foams Prepared with Oil-Phase Soluble Porogenic Solvents: Span 80 as Surfactant

Andrea Barbetta† and Neil R. Cameron*

Department of Chemistry, University of Durham, South Road, Durham, DH1 3LE, U.K.

Received December 18, 2003; Revised Manuscript Received February 17, 2004

ABSTRACT: Poly(divinylbenzene) emulsion-derived (PolyHIPE) solid foams prepared with porogens (toluene, chlorobenzene, (2-chloroethyl)benzene, 1,2-dichlorobenzene, and 1-chloro-3-phenylpropane) in the oil phase have morphologies and surface areas that are strongly influenced by the nature of the porogen. For the case where the surfactant employed is Span 80, we show that the solid foam structure depends on (i) the ability of the solvent to swell the growing network, (ii) the solvent polarity, and (iii) the ability of the solvent to adsorb at the emulsion interface. In particular, relatively polar solvents that are able to transport water through the emulsion continuous phase (Ostwald ripening) are shown to produce much lower surface areas than analogous resins prepared by homogeneous solution polymerization of divinylbenzene in the presence of the solvent in question alone. The influence of Ostwald ripening is further suggested by the observation that surface area decreases with increasing emulsion aqueous phase content for relatively polar solvents whereas little variation in surface area with aqueous phase content is observed for more hydrophobic solvents. All PolyHIPEs prepared were characterized by SEM, TEM, N_2 sorption analysis, and mercury intrusion porosimetry. The relative merits of TEM and mercury intrusion porosimetry as techniques for the reliable characterization of the solid foams are discussed.

Introduction

High internal phase emulsions (HIPEs) are two-phase liquid−liquid systems in which one of the phases, the internal or droplet phase, makes up more than 74% of the emulsion volume.[1] The heterogeneous structure can be used as a template for the production of a variety of materials with different morphologies. For example, curing of the droplet phase leads to agglomerates of particles, which have been studied extensively by Ruckenstein and co-workers.[2] Conversely, solidification of the continuous, or nondroplet, phase produces porous materials since polymerization occurs around and between the emulsion droplets.[3] Depending on conditions,[4] the droplets can either remain trapped within the solid matrix or can be removed, resulting in closed- and open-cell solid foams, respectively. The latter type of material is arguably the most interesting from an applications point of view; such materials have been termed PolyHIPE and have been the subject of considerable study. The morphology of these solid foams is determined by the structure of the emulsion prior to the gel point and so is dependent on emulsion stability as defined by such factors as surfactant type and content, temperature, composition of the emulsion phases, preparation conditions, e.g., shear rate, and so on. A number of articles describing the variation of structural features of the solid foams, including void and window size (vide infra for definition of terms) by control of emulsion stability have been published.[4−7]

Another structural feature that is useful to be able to control is the surface area. PolyHIPEs have relatively low surface areas (3−20 $m^2\ g^{-1}$ are typical) which hampers their applicability in areas such as heterogeneous catalysis, liquid chromatography and solid-phase extraction. However, much higher values can be obtained by replacement of some of the monomeric continuous phase with non-polymerizable solvent (porogen).[8,9] During polymerization, phase separation occurs within the developing polymer structure between the internal phase droplets. This leads to materials with dual porosity: very large macropores typical of PolyHIPEs, with pore diameters upward of 1 μm, and much smaller pores within the PolyHIPE walls. These latter pores are typical of those found in permanently porous resin beads, and indeed the pore size distribution obtained (micro-, meso- or macropores[10]) depends on the nature of porogen and amount of cross-linker used, as is the case for porous resins.[11] (The term "macroporous" is avoided here as it implies pores of diameter >50 nm.[10]) In a previous paper,[9] we described the influence of the porogen used to prepare poly(divinylbenzene) PolyHIPE materials on the resulting surface area and porosity. All porogens employed were "good" solvents for poly(DVB), yet large variations in both surface area and morphology were observed. We ascribed the differences in surface area to the solubility parameters of the porogens, while morphological effects were put down to adsorption of the porogens at the emulsion interface to varying extents. However, we have found subsequently that the situation is somewhat more complex. In the present article we present a fuller explanation for the influence of a given porogen on the structure of poly(DVB) PolyHIPE. In particular, it is suggested that Ostwald ripening plays a key role in the determination of the final solid foam structure.

Experimental Section

Materials. Divinylbenzene (Aldrich; 80 vol % *m*- (55 vol %) and *p*-divinylbenzene (25 vol %), the remainder being *m*- and *p*-ethylstyrene) was purified by passing through a column of basic alumina (Brockmann I) to remove the inhibitor (*p*-*tert*-butylcatechol). Toluene (T), chlorobenzene (CB), (2-chloroeth-

* Corresponding author. E-mail: n.r.cameron@durham.ac.uk.
† Present address: Dipartimento di Chimica, Università degli Studi di Roma, "La Sapienza", P.le A. Moro 5, 00185 Rome, Italy.

10.1021/ma0359436 CCC: $27.50
Published on Web 04/02/2004

yl)benzene (CEB), 1,2-dichlorobenzene (C_2B), 1-chloro-3-phenylpropane (CPP) (Aldrich), potassium persulfate (Aldrich), sorbitan monooleate (SPAN 80, Aldrich) and calcium chloride dihydrate (Avocado) were used as supplied.

PolyHIPE Preparation. The solid foams prepared were nominally 75, 85, 90, and 92% porous, based on aqueous phase content. The preparation method has been described elsewhere.[9] Briefly, the emulsions were obtained by adding dropwise an aqueous solution of $CaCl_2 \cdot 2H_2O$ (1.11 wt %) and potassium persulfate (0.22 wt %) to the organic phase, made of DVB 80% and SPAN 80 (20 vol % relative to total monomer plus porogen volume) under stirring. The polymerization was carried out at 60 °C in an oven for 48 h. The solid foams were extracted with water then 2-propanol for 24 h each in a Soxhlet apparatus. Solid foams were dried under vacuum at 50 °C to constant mass.

PolyHIPE Coding System. The PolyHIPE materials are classified by a code which is dependent on the monomers and cross-linker used to prepare the polymer, its cross-link density and pore volume. The codes for the basic poly(styrene−DVB) systems have the general form X*a*PV*b*(*z*Por)Surf, where X is the nominal cross-link density which corresponds to the actual concentration of DVB contained in the commercial products used (80%), PV is the nominal pore volume, as determined by the aqueous phase content, as a percentage, Por indicates the porogen which is present in the organic phase of the emulsion and whose concentration is referred to the volume of the monomer plus cross-linker (*z*) and Surf is the surfactant employed in emulsion preparation. Thus, X20PV90(1T)S80 would represent a poly(styrene−DVB) PolyHIPE material of approximately 20% cross-linker content, 90% pore volume, containing toluene as the porogen (1:1 vol:vol, monomer plus cross-linker to porogen) and prepared using SPAN 80 as the surfactant.

Bulk Polymerization. The polymerization of DVB 80% was carried out in the presence of toluene, chlorobenzene, 1,2-dichlorobenzene, (2-chloroethyl)benzene and 1-chloro-3-phenylpropane respectively, as diluents (monomer:porogen, 1:1 (v:v)). The polymerization reactions were carried out at 60 °C in 30 mL glass vials in a temperature-controlled oil bath for 24 h. AIBN was used as initiator (1 wt % relative to DVB 80%). The prepared bulk samples were crushed into powders and washed in a Soxhlet apparatus for 24 h each with THF and acetone. The polymers were dried in a vacuum oven for 48 h at 50 °C. The samples were analyzed by mercury intrusion porosimetry, N_2 adsorption, and SEM.

Surface Area/Pore Size Distribution. Nitrogen adsorption/desorption measurements were performed at 77.3 K on a Micromeritics TriStar 3000 model gas adsorption analyzer. Samples were degassed at 100 °C overnight under vacuum prior to data collection. Surface area measurements utilized a nine points adsorption isotherm collected over 0.05−0.20 P/P_0 and the data were analyzed via the BET method.[12] For each sample a minimum of six determinations were carried out and results are expressed as averages with the associated standard deviations. The average pore size distributions utilized a 53-point adsorption isotherm and were analyzed via the BJH method in accordance with procedures from the British Standards Institution.[13] Micropore volumes and areas were evaluated via the *t*-plot method.

Mercury Intrusion Porosimetry. Mercury intrusion porosimetry analysis was performed using a Micromeritics AutoPore III 9420. Samples were outgassed under vacuum at room temperature for 30 min before intrusion. Intrusion and extrusion mercury contact angles of 130° were used; measurements were conducted according to the set-time equilibration mode. Penetrometers with a stem volume of 1.1310 mL were used. The intrusion volume always comprised between 50 and 85% of the stem volume. Intrusion pressures for PolyHIPEs never exceeded 200 psi (1.38 MPa) in order to avoid any specimen compression; up to 60 000 psi (413.7 MPa) was used in experiments involving polyDVB permanently porous resins.

Electron Microscopy. A Hitachi S2400 electron microscope operating at 25 kV was used for studies of the morphology of the samples. Prior to analysis, specimens were sputter coated with a thin layer of gold to enhance conductivity. Samples for TEM were fixed in 1% aqueous OsO_4 solution and dehydrated in a graded series of alcohols, then embedded in Emix (medium) Resin TO28 (TAAB Laboratories Equipment Ltd.). Curing of the resin was carried out for 36 h at 60 °C. Ultrathin sections (90 nm) of the resulting composite were cut using a Diatome 45 diamond knife (TAAB Laboratories Equipment Ltd.) on a Ventana (RMC) MT-XL Ultramicrotome (Ventana Medical System Inc.). The sections were mounted on uncoated 400 mesh copper Gilder grids G400, of 3.05 mm diameter. The grids were examined using a Philips CM100 (compustage) transmission electron microscope (TEM) operated at 100 kV. Micrographs were recorded at magnifications of 380, 4600 and 10 500×. Micrographs taken at 380× were used for the evaluation of the average void and interconnecting window diameters. Such measurements were carried out using the instrument software on a significant number of voids (typically, a few hundred) in order to give statistical relevance to the figures produced.

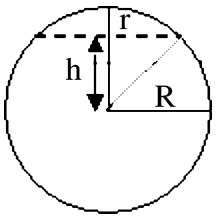

Figure 1. Schematic of a void or interconnecting window. Key: *R*, equatorial value of the radius of a sphere or circle; *r*, value of the radius of a circular section at a distance *h* from the center of the sphere.

Average diameters measured in this way are underestimates of the real values as the sectioning of specimens carried out with the ultramicrotome samples voids at a random distance from the void center. Therefore, it is necessary to introduce a statistical correction. This is accomplished by evaluating the average of the ratio R/r, where R is the equatorial value of void diameter and r is the diameter value measured on the micrographs (Figure 1).

This statistical factor is calculated as follows: h is related to r and R according to eq 1:

$$h^2 = R^2 - r^2 \tag{1}$$

The probability that the sectioning takes place at any distance (h) from the center is the same for all values of h, so the average probability value of h is $R/2$.

By replacing this value in eq 1 we get $R/r = 2/(3^{1/2})$. Multiplication of the observed average value of the diameter and interconnecting window by this factor allows a better estimation of the real void diameter to be obtained.

Results and Discussion

PolyHIPEs. The surfactant most commonly employed in the production of W/O HIPEs is sorbitan monoleate (SPAN 80, HLB = 4.2), which is insoluble in water (low HLB value surfactants are hydrophobic) so, it was natural to use this surfactant in the production of our solid foams. The HIPEs were prepared with 20% (w/v) surfactant concentration relative to the continuous phase (minus surfactant), using procedures described in the Experimental Section. No difficulties were encountered, and all HIPEs were stable up to the point of gelation. Therefore, the changes in structure discussed in the forthcoming section are not due to emulsion breakdown. As the morphology of the materials is quite complex, it is worthwhile at this point to define some of the terminology that will be used in the subsequent discussion. The large (on the order of microns) spherical voids in the materials (see Figure 2) are termed voids. (The previously used term "cells" was dropped to avoid

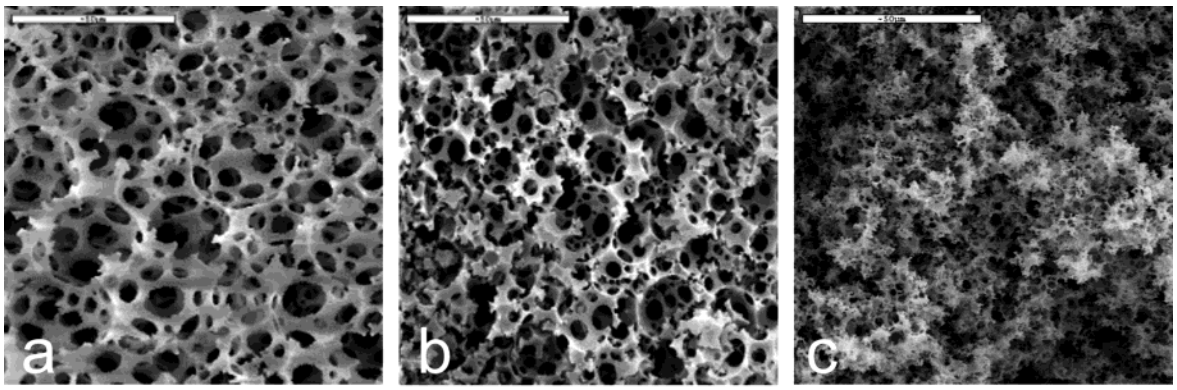

Figure 2. SEMs of PolyHIPEs prepared with porogens: (a) T; (b) C_2B; (c) CPP. Scale bar = 50 μm.

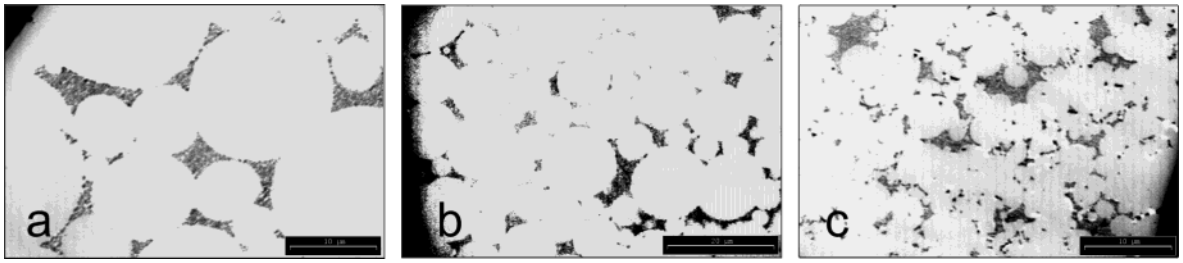

Figure 3. TEMs of PolyHIPE materials: (a) X80PV90(1T)S80; (b) X80PV90(1C_2B)S80; (c) X80PV90(1CPP)S80. Scale bar = 10 μm ((b) = 20 μm).

confusion during work involving cell culturing on PolyHIPE scaffolds;[14] for consistency, we prefer to keep the term "voids" .) The interconnects between adjacent voids are referred to as windows. Finally, the use of inert porogens in the monomer phase results in the formation of pores within the polymer phase. These may be micro-, meso-, or macropores, according to their size as defined by IUPAC.[10]

Examination of SEMs at low magnification (Figure 2) indicates an influence of the porogen type on the solid foam morphology on a large scale. Changing from T (Figure 2a) to C_2B (Figure 2b) causes a marked decrease in void diameter. It is well-known that droplet size decreases with increasing emulsion stability since the surface energy per unit area is lower. A decrease in emulsion droplet size leads to a decrease in PolyHIPE void size since the solid foam is effectively a replica of the emulsion structure immediately prior to gel formation. Figure 2c provides further information about the influence of porogen on solid foam morphology, and suggests that the characteristic open-cellular PolyHIPE structure is absent when the porogens are CPP or CEB (latter not shown). The morphology of this material resembles more closely that of monoliths prepared by Svec and Fréchet,[15] albeit with higher porosity. It is conceivable that the HIPE has collapsed prior to polymer gelation, resulting in a noncellular structure, however no evidence of emulsion breakdown such as separated aqueous phase was observed. We wondered whether this morphology transition could be due to an influence of the porogen on the size of the windows connecting adjacent voids, in addition to an influence on void size. If the window diameter increased to a sufficiently high extent, only polymer struts would remain, giving the impression of a loss of cellular structure. This hypothesis is supported also by Figure 2b, referring to a PHP prepared by including C_2B in the organic phase. Its morphology represents a transition between those of X80PV90(1T)S80 and X80PV90(1CPP)-S80. The typical PolyHIPE open-cellular morphology is still evident, but the walls have lost some of their structural integrity resulting in the appearance of some strut structure.

Williams and co-workers[6] observed a loss of cellular structure at very high surfactant levels (75% relative to total oil phase including surfactant) for poly(S-DVB) PHPs, although this was not rationalized fully. Also reported in that work, and separately by workers at Unilever,[16] was an increase in window size as the concentration of electrolyte in the aqueous phase was increased. Both these observations imply that window size increases as the interfacial tension decreases. The explanation is that as the interfacial tension decreases, the films separating adjacent emulsion droplets become thinner. Previously, using cryo-SEM experiments,[17] it was shown that the point at which the windows appear coincides with the polymerization gel point, implying that shrinkage due to the conversion of monomer to higher density polymer is the probable cause of window formation. A thinner film undergoing shrinkage would result in a larger window, and one can imagine that if the windows were very large the cellular structure would not be obvious. Further evidence for this is provided by TEM at low magnification (×380) of the solid foams prepared with T, C_2B, and CPP (Figure 3), which indicates that the cellular morphology has indeed been retained and that the original spherical droplets merge to a greater extent when the porogenic solvent is changed from T to C_2B or CPP. TEM shows much more clearly the retention of the cellular structure than the corresponding SEM (compare Figures 2c and 3c), and proves that the HIPE has been stable up to the gel-point.

A quantitative description of the morphology of the solid foams in terms of the average void ($\langle D \rangle$) and interconnecting window ($\langle d \rangle$) diameters, as well as the degree of interconnection as expressed by their ratio ($\langle d \rangle / \langle D \rangle$), provides useful information on the structure of the

Table 1. Characterization of PolyHIPE Solid Foams

sample[a]	$\langle D\rangle$ (μm)[b]	$\langle d\rangle$ (μm)[c]	$\langle d\rangle/\langle D\rangle$	sample characteristics
X80PV90(1T)S80	11.5	4.0	0.35	chalky; moderately tough
X80PV90(1CB)S80	9.8	4.5	0.46	chalky; moderately tough
X80PV90(1C_2B)S80	7.4	3.7	0.50	chalky; moderately tough
X80PV90(1CEB)S80	not determinable			crumbles easily into fine powder
X80PV90(1CPP)S80	not determinable			crumbles easily into fine powder

[a] See Experimental Section for sample coding system. [b] Average void diameter. [c] Average interconnecting window diameter.

Table 2. Surface Areas, Cumulative Pore Volume, Average Pore Diameter, Micropore Volume, and Micropore Areas of DVB 80% PolyHIPE Solid Foams

sample[a]	surface area (m^2/g)[b]	V_p (cm^3/g)[c,d]	$\langle D_w\rangle$ (nm)[c,d]	micropore vol (cm^3/g)[e]	micropore area (cm^2/g)[e]
X80PV90(1T)S80	359 ± 10	0.44 ± 0.02	6.4 ± 0.1	0.022 ± 0.001	59 ± 3
X80PV90(1CB)S80	346 ± 26	0.68 ± 0.05	8.4 ± 0.6	0	0
X80PV90(1C_2B)S80	499 ± 18	0.85 ± 0.02	6.7 ± 0.2	0.019 ± 0.003	59 ± 7
X80PV90(1CEB)S80	432 ± 19	0.72 ± 0.04	7.0 ± 0.3	0	0
X80PV90(1CPP)S80	435 ± 20	0.74 ± 0.04	7.0 ± 0.2	0	0
X80PV75(1CB)S80	457 ± 8	0.66 ± 0.05	6.0 ± 0.2	0.0076 ± 0.0002	55 ± 6
X80PV85(1CB)S80	472 ± 3	0.77 ± 0.03	6.2 ± 0.2	0.015 ± 0.002	48 ± 5
X80PV92(1CB)S80	236 ± 11	0.65 ± 0.03	11.2 ± 0.2	0	0
X80PV90(0.5CB)S80	375 ± 28	0.52 ± 0.04	6.3 ± 0.5	0.25 ± 0.007	65 ± 15
X80PV90(0.5CEB)S80	157 ± 24	0.33 ± 0.03	8.7 ± 0.6	0	0
X80PV75(1CEB)S80	367 ± 6	0.54 ± 0.01	6.2 ± 0.2	0	0

[a] See Experimental Section for sample coding system. [b] From BET treatment of N_2 adsorption data. [c] See text for definition of terms. [d] From BJH treatment of N_2 adsorption data. [e] From *t*-plot.

emulsion prior to gelation. This in turn depends on the physical parameters of the emulsion, one of the most important of which is the interfacial tension. A relatively low interfacial tension value will favor the dispersion of the internal phase because the work required to break droplets into smaller ones is relatively low. This translates into the formation of voids of smaller dimension. The three-dimensional packing of such an array of droplets will be more compact, the O/W interfacial area will be higher and as a consequence the thickness of the layer of continuous phase surrounding droplets of the dispersed phase will be thinner. On polymerization of the continuous phase, this will lead to the formation of larger windows, relative to void dimension. Thus, the values of the ratio $\langle d\rangle/\langle D\rangle$ is strictly connected with the degree of thinning of the continuous phase film separating droplets of the dispersed phase. Measurements of $\langle d\rangle$ and $\langle D\rangle$ are best carried out from TEM micrographs taken at low magnification where the complex morphology of the PolyHIPE is projected in 2D. A statistical correction was used in order to compensate for the underestimation of values produced by direct measurement (see Experimental Section).

In Table 1, the values of $\langle d\rangle$ and $\langle D\rangle$ are reported for the solid foams produced with different porogens with the exception of CEB and CPP because in these cases the extensive overlapping among voids made reliable measurements difficult. As can be seen, the average void diameter, $\langle D\rangle$, decreased markedly on changing porogen from T to CB and C_2B. The decrement of $\langle d\rangle$ is not proportional to but tends to lag behind $\langle D\rangle$ with the consequence that the ratio $\langle d\rangle/\langle D\rangle$ increases down the porogens listed in Table 1, indicating that voids tend to overlap to an increasing extent. These data further support the hypothesis outlined above, regarding the progressive thinning of the films of the continuous phase surrounding droplets when the porogen is changed from T to CB, C_2B, and, presumably, CEB and CPP.

As stated above, in the case of X80PV90(1CEB/CPP) it was not possible to provide quantitative data for $\langle d\rangle$ and $\langle D\rangle$ but qualitative inspection and comparison among micrographs (Figure 3a−c) clearly shows that the degree of interconnection is higher than any other.

The degree of interconnection is reflected by the mechanical properties of the solid foams prepared with different porogens (Table 1). Thus, as $\langle d\rangle/\langle D\rangle$ increases the materials become weaker and tend on drying under vacuum to undergo collapse to an increasing extent. This is also clearly visible from inspection of SEM micrographs (Figure 2a−c): the PolyHIPE prepared with T as porogen maintains entirely its structural integrity; that prepared with C_2B shows some degree of damage; that prepared with CPP clearly suffers substantial damage. The differences among $\langle d\rangle/\langle D\rangle$ values might be a direct consequence of the lowering of the O/W interfacial tension at the emulsion stage, determined by the nature of the porogen employed as all the other components of the emulsion are the same. According to this hypothesis the lowering of interfacial tension caused by the porogens used should follow the order: T < CB < C_2B < CEB ≈ CPP. We have previously shown,[9] on a semiquantitative basis by using a Langmuir trough, that the degree of adsorption at the water/air interface of organic mixtures containing DVB, SPAN 80, and the porogens employed in this study followed the same order indicated above. Therefore, these data seem to confirm the suggestion that the apparent loss of cellular structure observed in X80PV90-(1CEB/CPP)S80 is due to extremely large interconnecting windows appearing due to excessive thinning of surfactant films between adjacent emulsion droplets, as a result of a progressive lowering of interfacial tension as the solvent becomes a better cosurfactant for the emulsion.

The surface areas and porosity data (plus associated errors in their measurement) for the solid foams prepared with the five porogens, are reported in Table 2. V_p is the cumulative pore volume as determined by N_2 adsorption and $\langle D_w\rangle$ is the average diameter of small pores within the walls of the solid foams. In Figure 4a, an example of a N_2 adsorption/desorption isotherm showing the hysteresis loop encountered with these solid

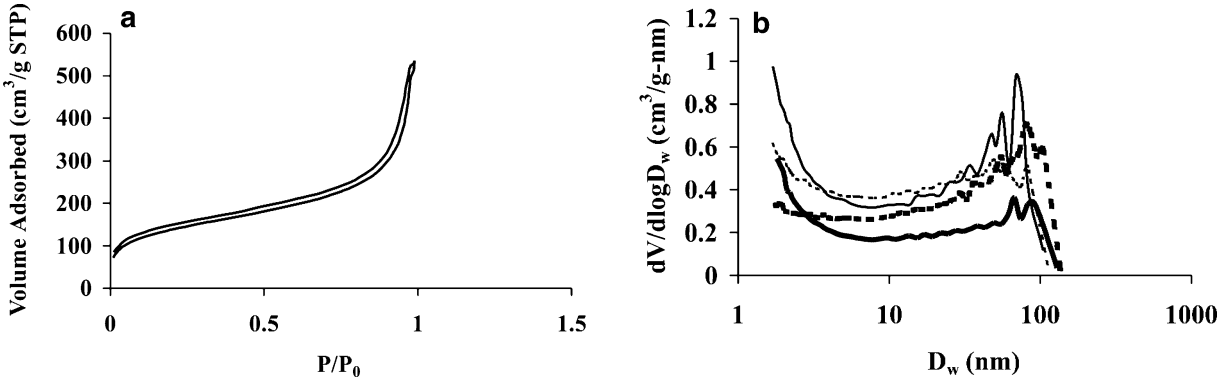

Figure 4. (a) example of N_2 isotherm encountered with solid foams listed in Table 1; (b) pore size distributions (BJH) of X80PV90-(1Por)S80 PolyHIPE solid foams calculated from the adsorption branch of the isotherms. Porogens used: T (heavy line), CB (heavy broken line), C_2B (solid line), and CPP (broken line). Data for CEB are almost coincident with those for CPP and have been omitted for clarity. See text for porogens key.

foams is displayed. All solid foams exhibit a type II isotherm and type H4 hysteresis loop.[18] Pore size distribution curves are shown in Figure 4b. All distributions are quite broad, spanning a range in pore diameter of 2 orders of magnitude, and all exhibit a significant proportion of macropores (>50 nm). The combination of a narrow hysteresis loop and broad pore size distributions is indicative of good pore connectivity.[18] In idealized porous matrices with good pore connectivity, a small hysteresis loop is often associated with a narrow pore size distribution and a large hysteresis loop with a broad distribution. Simplistically, poor or low pore connectivity would lead to large hysteresis effects and very high connectivity to low hysteresis.

Surface area data (Table 2) show a clear dependence on the nature of the porogen. Solid foam samples can be divided into three sets: those with relatively low (entries 1 and 2), intermediate (entries 4 and 5), and high surface areas (entry 3). X80PV90(1T)S80 and X80PV90(1CB)S80 have very similar surface areas even though the comparison of the other porosimetry data and pore size distributions reveal that the pore structure is quite different (Table 2 and Figure 4). Differences between solid foams prepared with T and CB arise mainly from the relative proportion of macro- (>50 nm) and mesopores (2−50 nm). The pore size distribution of solid foams prepared with T rises above that of solid foams from CB in the lower side of the mesopore region and 17% of the surface area is due to the presence of micropores, while the latter is characterized by a higher amount of macropores and as a result these solid foams possess a higher pore volume and average pore diameter (Table 2, entries 1 and 2). Porosity data from the second group of solid foams (Table 2, entries 4, 5) are coincident within experimental error. This is not surprising considering the similarity of the chemical structures of the porogens (CEB and CPP) employed in the preparation of such solid foams. The solid foam prepared with C_2B has the highest surface area and pore volume. The micropores contribute to the surface area to an extent of 12%. The pore size distribution of the solid foam prepared with C_2B is characterized by a higher content of both macro- and mesopores as compared to the previous solid foams and as a result its surface area and pore volume are the highest. Surface area data seem to indicate that C_2B is the porogen with the best solvating characteristics for poly(DVB80%).

Porosity data and pore size distributions determined by means of N_2 adsorption are confirmed on a qualitative basis by SEM and TEM pictures taken at high magnification (Figure 5, left and right column, respectively). For instance, the SEM of X80PV90(1T)S80 (Figure 5a) shows that the microstructure is formed by relatively large aggregates of gel microparticles: spaces between agglomerates of these aggregates are responsible for the presence of macropores (>50 nm) as is evident from TEM micrographs (Figure 5b). Smaller mesopores (2−50 nm) arise from spaces within single aggregates and gel microparticles. Micropores (<2 nm) are located within nuclei forming a gel microparticle.[11,19] On the contrary, in the case of solid foams prepared from CEB, microgel particles self-organize in clusters of smaller and less polydisperse dimensions (Figure 5c) and as a result the porosity is more homogeneous

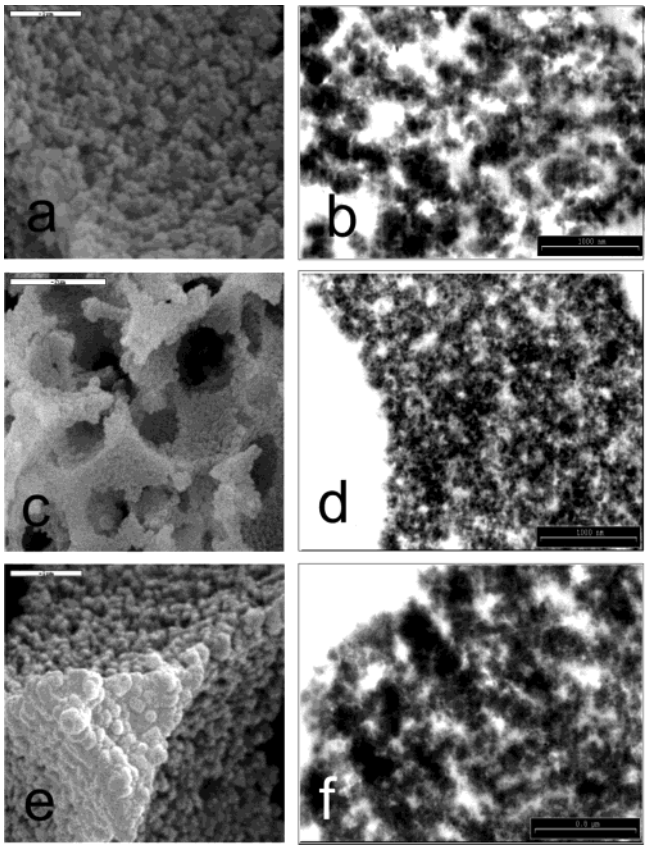

Figure 5. SEMs (left column) and TEMs (right column) of PHPs prepared with porogens: (a and b) T; (c and d) CEB; (e and f) C_2B. Scale bars: (a and c) 2 μm; (b, d, and e) 1 μm; (f) 0.8 μm.

Table 3. Solubility Parameters of the Solvents Used as a Porogens in the Preparation of PolyHIPEs and in the Bulk Polymerization of DVB 80%

porogen	δ_t $(MPa)^{1/2}$	δ_d $(MPa)^{1/2}$	δ_p $(MPa)^{1/2}$	δ_h $(MPa)^{1/2}$
T[23]	18.2	18	1.4	2.0
CB[23]	19.4	19	4.3	2.0
C_2B[23]	20.5	19.2	6.3	3.3
CEB[a]	20.3	18	7.7	3.9
CPP[a]	20.0	18.1	6.8	3.5
water[23]	47.9	15.5	16.0	42.4

[a] Values calculated by the method of Hoftyzer−van Krevelen and Hoy, and average taken.[24]

(Figure 5d). X80PV90(1C_2B)S80 porosity seems to be more polydisperse than those of X80PV90(1CEB)S80 but less so than X80PV90(1T)S80.

Differences in surface area and porous structure show that the porogens used have different solvating powers toward poly(DVB80%). A criterion used widely to evaluate the quality of a solvent for a polymer is the three-dimensional solubility parameter δ_t,[20,21] which comprises contributions from dispersive, δ_d, dipolar, δ_p, and hydrogen bonding, δ_h, interactions. In a three-dimensional diagram the porogen and polymer can be represented by two points, and the porogen−polymer affinity can be described by the distance d_0 between these two points.[20]

$$\delta_t^2 = \delta_d^2 + \delta_p^2 + \delta_h \quad (2)$$

$$d_0^2 = 4(\delta_{d1} - \delta_{d2})^2 + (\delta_{p1} - \delta_{p2})^2 + (\delta_{h1} - \delta_{h2})^2 \quad (3)$$

The indices 1 and 2 represent the porogen and polymer, respectively. Although many of these cohesion parameters, such as the Hansen or Hoy parameters,[22] are tabulated in the literature, we are faced with the rather common problem that data for not all the porogens, and none of the polymers, are available. The values of the three-dimensional cohesion parameters of T, CB, and C_2B were taken from the literature;[23] those of CEB and CPP were calculated by applying a group contribution method according to Hoftyzer-van Krevelen and Hoy[24] (both methods are of the same accuracy, and it has been suggested that these should be averaged[24]). The three-dimensional solubility parameters and their components for the five solvents are given in Table 3. As can be seen, δ_t reaches its maximum value with C_2B. Furthermore, δ_p and δ_h increase steadily from T to CEB and CPP.

Poly(styrene−divinylbenzene) (PDVB) permanently porous resins have been prepared using a wide range of porogens, including swelling and nonswelling solvents (as individual components or mixtures)[21,25] and linear polymers.[26] The solubility parameter value (δ) for PS-DVB quoted in the literature[23] is 18.6 $(MPa)^{1/2}$. The literature[20] defines good solvents with $d_0 < 10.0$, intermediate solvents with $10.0 < d_0 < 12.7$, and bad solvents with $d_0 > 12.7$. All porogens used are very good solvents, their solubility parameters being between 18.2 and 20.5 $(MPa)^{1/2}$. According to the values of δ_t, T should be the best solvent and, as a consequence, when used in preparing solid foams should produce materials with the highest surface area. The surface area results, on the contrary, show that the highest surface area is obtained in conjunction with C_2B whose solubility parameter (Table 3) is the most distant from that of PSDVB. In practice the level of cross-linker employed also influences the onset of phase separation and for some commercially produced S-DVB resins, the DVB level is adjusted upward such that even with toluene, a thermodynamically good solvent for polystyrene, as a porogen, phase separation occurs eventually, since pure poly(DVB) is less compatible with toluene than is polystyrene itself. Thus, it is to be expected that the real value of δ for poly(DVB 80%) is higher than 18.6 $(MPa)^{1/2}$ quoted for polystyrene. The increase in polarity and hydrogen bond forming ability as witnessed by values of δ_p and δ_h matches well with the O/W interfacial behavior exhibited by these molecules as evidenced by $\langle d\rangle/\langle D\rangle$ values (Table 2). In the literature[27] it has been reported that aromatic molecules have the capability of penetrating the surfactant monolayer at the interface and that this property is enhanced by the polarity and hydrogen bond formation ability of such molecules.[28]

While the correlation between the solid foam morphology ($\langle D\rangle$, $\langle d\rangle$, $\langle d\rangle/\langle D\rangle$), and porogen physical properties (δ_t, δ_d, δ_p, δ_h) is quite evident, that regarding their swelling properties toward poly(DVB 80%) is not clear. There are two possible reasons for this situation: (i) the solubility parameter of poly(DVB 80%) is not known; (ii) the structure of concentrated, polymerizable, emulsions is complex. High internal phase emulsions of the type employed in the present study consist of two isotropic liquid phases: one, the droplet phase, is a submicellar surfactant solution in water, and the other, the continuous phase, is a swollen reversed solution or water-in-oil (W/O) microemulsion.[29] Since the surfactant aggregates formed are microemulsions, the critical concentration of surfactant required for their formation is referred to as the critical microemulsion concentration (cμc). For nonionic surfactants the cμc in oil is typically on the order of 0.1 M whereas the value in the corresponding aqueous phase is on the order of 10^{-5} M. The oil−water interfacial tension (γ) reaches a virtually constant value above the cμc.

The presence of such inverse micelles in the continuous phase has been used to capture monomer-insoluble diluents such as water inside the organic phase. Thus, the cross-linking copolymerization in the continuous phase of a water-in-oil microemulsion also yields a macroporous network.[30] The nature of the porous structure is largely dependent on the microstructure of the microemulsion.[31] Short chain alcohols have been used as cosurfactants together with conventional surfactants for the production of microemulsions.[32] For instance, it was shown that the water solubilized in reverse micelles can be used as a diluent in the production of porous S-DVB copolymer beads by suspension polymerization. In this technique, sodium bis(2-ethylhexyl)sulfosuccinate (AOT) was used as the surfactant for the formation of reverse micelles: depending on the amount of water solubilized in the micelles, the size of the water droplets inside the S-DVB monomer mixture is different. Thus, the size of the pores is controlled by adjusting the water content in the reverse micelles prior to polymerization.[33,34]

Surface areas obtained in this way are usually rather low: for instance Xhu et al.[33] obtained porous materials characterized by surface areas not higher than 30 m^2 g^{-1}. Hainey et al.[8] measured for X20PV90 (no porogen) a surface area value of about 22 m^2 g^{-1} using a concentration of SPAN 80 of 34% w/v. These values of surface areas are lower than the differences found in

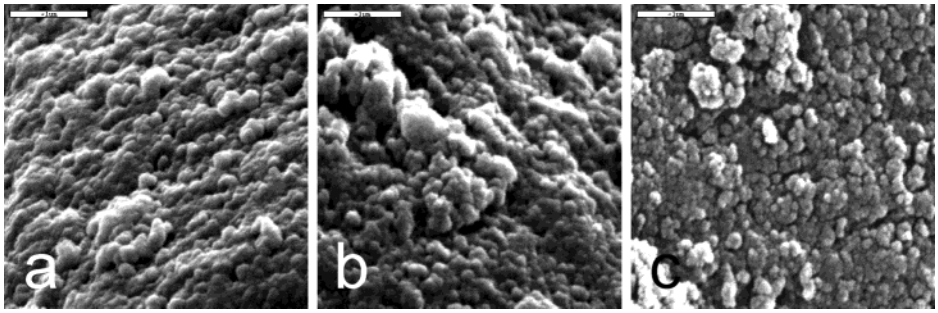

Figure 6. SEMs of DVB 80% permanently porous resins obtained by bulk polymerization and using different porogens: (a) T; (b) C_2B; (c) CPP (see text for key). Scale bar = 1 μm.

Table 4. Nitrogen Adsorption and Mercury Intrusion Porosimetry Results for DVB 80% Monoliths Obtained in the Presence of Different Porogenic Solvents

sample	surface area (m^2/g)[a]	vol of pores between 2 and 200 nm (cm^3/g)[b]	vol of pores between 3 and 1000 nm (cm^3/g)[c]	$\langle D_b \rangle$ (nm)[b,d]	micropore vol (cm^3/g)[e]	micropore area (cm^3/g)[e]
DVB80(T)	760 ± 8	0.891 ± 0.008	0.736	4.515 ± 0.008	0.0057 ± 0.0004	40 ± 1
DVB80(CB)	781 ± 9	0.982 ± 0.009	0.838	4.92 ± 0.02	0.0173 ± 0.0006	64.0 ± 0.4
DVB80(C_2B)	829 ± 7	1.09 ± 0.01	0.9317	5.08 ± 0.01	0.0118 ± 0.0003	54.6 ± 0.7
DVB80(CEB)	799 ± 1	1.159 ± 0.003	0.981	5.66 ± 0.01	0.0126 ± 0.0007	55 ± 1
DVB80(CPP)	783 ± 2	1.219 ± 0.008	1.07	6.07 ± 0.05	0.0123 ± 0.0004	54 ± 1

[a] From BET treatment of N_2 adsorption data. [b] From BJH treatment of N_2 adsorption data. [c] From Hg intrusion porosimetry data. [d] See text for definition. [e] From *t*-plot.

our solid foams. There is another aspect which tends to rule out microemulsion templating as an important factor contributing to the surface areas of our solid foams: the polarity of the medium. Binks et al.[35] showed that when the polarity of the medium in which the surfactant is dissolved is changed from apolar, such as heptane, to more polar, such as a 1:1 vol:vol mixture of heptane and medium chain length triglyceride, the surfactant cμc increased from 3.0 to 10.3 wt %. They have also discovered a strong dependence of post cμc tension (γ_c) on temperature, a variation of about 10 °C causing a 2-fold increase of γ_c.

On the basis of these findings, we would expect the number of inverse micelles inside the continuous phase to decrease as the porogen is changed from T to CEB or CPP because, as is evident from Table 3, the polarity of these porogens increases. As a consequence, SPAN 80 cμc should increase in the same order and microemulsion templating should contribute to the overall porosity and surface area to a lesser extent. Experimentally, we do not observe a trend that correlates polarity with surface areas: the highest surface area is obtained using as a porogen C_2B, whose polarity is midway between those of T and CPP. Furthermore, the surface areas obtained by employing relatively polar porogens (CEB, CPP) are higher than those with a lower polarity porogen (T). Thus, while we cannot rule out a contribution to total solid foam porosity arising from the presence of microemulsion W/O droplets in the organic phase, this effect is unlikely to be able to explain the differences in surface areas in the series of solid foams described. Concentrated emulsions are heterogeneous systems: the two phases are not static, noninteracting systems but, depending on the nature of the surfactant layer at the interface, may undergo partitioning and diffusion of the dispersed phase through the continuous one (Ostwald ripening, see later sections).

Permanently Porous Resins from DVB 80%. The superimposition of all the effects described above, for a given porogen, makes it difficult to establish their relative contribution in determining the final morphology of a solid foam. With the aim of establishing an order of solvent quality toward poly(DVB 80%), we carried out the bulk polymerization of DVB 80% in the presence of the five porogenic solvents listed in Table 1 and investigated the structure of the obtained resins by SEM, nitrogen adsorption and mercury intrusion porosimetry. The values of surface areas of the resins are also useful in another respect: they allow us to establish an upper limit of PolyHIPE surface area values reachable with a porogen when used as an emulsion constituent. The comparison between the surface area of a resin and that of the corresponding PolyHIPE solid foam, both obtained using the same porogen, can give an indication of the extent of the cumulative effects exerted by partitioning and diffusion. In Figure 6, SEM images obtained for poly(DVB(T)), poly(DVB(C_2B)), and poly(DVB(CPP)) show clearly the globular structure of these materials. There are no discernible differences regarding size and aggregation state of microgels composing different resins.

Table 4 reports results obtained by N_2 sorption and mercury intrusion porosimetry. $\langle D_b \rangle$ is the average pore diameter of DVB 80% resins produced by bulk polymerization. For the first two resins (poly(DVB(T)) and poly(DVB(CB))) there are already data available in the literature.[36] Our values of surface areas are within less than 10% of the published ones. Regarding the influence of the other three chlorinated solvents, C_2B, CEB, and CPP, on the microstructure of poly(DVB), as far as can be determined, no data have been published so far. As can be seen, all solvents are very good porogens for poly(DVB 80%), porous resins with surface areas exceeding 700 $m^2\ g^{-1}$ being produced. It is evident from the data reported in Table 4 that surface areas pass through a maximum in the case of poly(DVB(C_2B)). This indicates that C_2B is the best porogen.

The pore volume behavior of the resins prepared is illustrated by both mercury intrusion porosimetry and N_2 adsorption results (Figure 7). Pore volumes follow

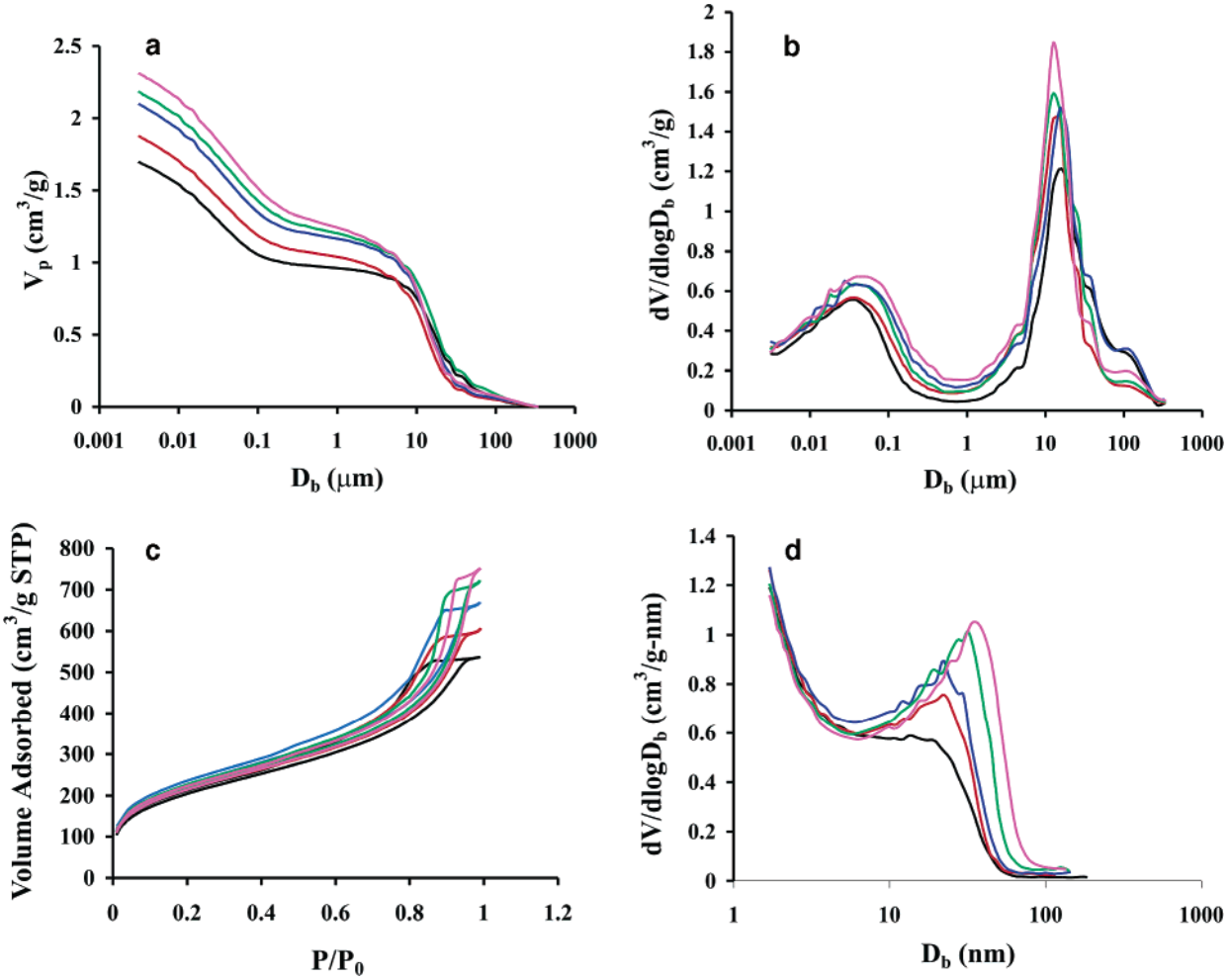

Figure 7. Cumulative pore volume (a) and pore size distributions (b), determined by mercury intrusion porosimetry, plus N_2 sorption isotherms (c) and BJH pore size distributions (d), determined by N_2 sorption, of DVB 80% resins obtained by bulk polymerization in the presence of different porogenic solvents: T (black); CB (red); C_2B (blue); CEB (green); CPP(magenta) (see text for key). See text for definition of D_b.

the order: T < CB < C_2B < CEB < CPP and reach the maximum value with poly(DVB(CPP)) (Figure 7b). This resin possesses the same surface area as poly(DVB(CB)) but its pore volume is about 20% higher.

Pore volumes obtained by mercury intrusion porosimetry are consistently lower than those provided by N_2 sorption (Table 4) and this may be a consequence of some collapse suffered by specimens because of the high-pressure applied (up to 60 000 psi). Mercury intrusion cumulative pore volume and pore size distribution plots (Figure 7, parts a and b, respectively) show the presence of two sets of pore size distributions: one covering the range in pore diameter between 5 and 300 μm the other below 5 μm. The former is clearly attributable to void space among particles of the powdered resins, the latter is due to the porous structure characterizing the resins themselves.

The N_2 sorption isotherms are complete and are of type IV[10] with a type H2 hysteresis loop.[18] The adsorption and desorption branches get closer when the porogen employed in resin preparation is changed from T to CPP and this is clearly an indication that the adsorption and evaporation processes take place in pores of increasing diameters as evident in Figure 7c. This is in agreement with data regarding average pore diameter and pore volumes which increase from T to CPP. In Figure 7d, BJH adsorption dV/d(log D_w) pore size distributions are reported. The pore size distributions of resins obtained by using as porogens T, CB, and C_2B cover the same diameter range. As can be seen, the position of the peaks is the same, the differences consisting of the relative heights in each case. In the case of resins obtained using CEB and CPP as porogens, the pore size distributions become increasingly broader and as a result, the positions of the peaks shift toward higher diameter values, the proportion of larger pores increases while that of the mesopores remains at a level comparable to that of poly(DVB(CB)). The set of N_2 adsorption results shown indicate that C_2B is, among those studied here, the solvent with the best swelling properties toward poly(DVB 80%). The correlation between δ (Table 3) and surface area data (Table 4) indicates that the solubility parameter of poly(DVB) should be very close to 20.5 (MPa)$^{1/2}$.

N_2 adsorption results for porous resins indicate that solvent quality is not the main factor responsible for the differences encountered among the PolyHIPE solid foams obtained by using the same set of porogens. In fact, in the former samples surface areas differ by less than 10%, while in the latter variations are much more pronounced. It is worth noting that the percentage contributions of micropores to the total surface areas for the permanently porous resins is much lower than in the corresponding PolyHIPE solid foams while pore

volumes are much higher. Furthermore, the combination of higher surface areas and pore volumes points to less polydisperse pore size distributions, as is evident also from comparison of their pore size distributions (Figures 4b and 7d). The difference in porous structure indicates that when polymerization is taking place within the emulsions, the reacting medium is a poorer solvent for the developing network than in the bulk mode. It should be pointed out that the poly(DVB) monoliths were prepared with an oil-phase soluble initiator (AIBN), whereas PolyHIPEs are synthesized using $K_2S_2O_8$ which is soluble in water. Despite the fact that each type of porous material is prepared under different conditions, we believe that useful information regarding the influence of a given porogen on the porosity of poly(DVB), in particular the maximum surface area achieveable with that solvent, has been obtained by preparing and characterizing the monoliths from bulk polymerization.

Influence of Pore Volume on Solid Foam Characteristics. To obtain further experimental evidence which could aid the interpretation of the results presented so far, we have investigated the influence of other emulsion composition variables, namely pore volume and monomer-to-porogen ratio, on solid foam porosity and surface areas. The effect of pore volume (PV) on the morphology (void size, interconnecting windows size and degree of void packing) of PolyHIPE solid foams obtained from DVB 80% and with CB as a porogen (monomer:porogen = 1:1) is illustrated by SEM and TEM micrographs in Figure 8. It is evident that the thickness of the walls separating voids depends strongly on PV and as a result the size of the interconnecting windows varies with PV. Because of the high organic/aqueous phase ratio at low PV the degree of overlapping among voids is limited (Figure 8, parts b and d) and the size of the interconnecting windows, especially in X80PV75(1CB)S80, is relatively small (Figure 8a). In the case of X80PV85(1CB)S80, the size distribution of the windows seems to be more polydisperse (Figure 8c). The morphology of X80PV92(1CB)S80 (Figure 8, parts g and h) is characterized by large voids and windows. The increase in PV is accompanied by thinning of the interfacial film separating emulsion droplets. On polymerization, shrinkage is more significant causing larger windows to appear.[17] Examination of TEM micrographs (Figure 8, parts b, d, f, and g) confirms the observations made from SEM micrographs and reveals some interesting additional features. For instance, the comparison between solid foams of PV 75 and 85 shows that voids in the latter are on the average more separated and tend to be grouped in clusters, leaving zones of the solid foam free of voids. This will turn out to be an important observation.

TEM micrographs taken at low magnification (×380) were used for the evaluation of the average void ($\langle D \rangle$) and interconnecting window ($\langle d \rangle$) diameters. The results are reported in Table 5. With the exception of X80PV75-(1CB)S80 (entry 1), both $\langle D \rangle$ and $\langle d \rangle$ increase with PV. Values of the ratio $\langle d \rangle / \langle D \rangle$ increase steadily along the series of solid foams indicating that overlapping among voids is occurring to an increasingly greater extent as PV is increased.

Another popular technique widely used for the investigation of porous materials is mercury intrusion porosimetry.[37] This technique is particularly useful to detect experimentally the existence of a continuous network of macropores. A peak in the macropore size range occurs only if the macropore network is continuous; otherwise the macropores are screened by smaller pores and are not detected. In the past, mercury intrusion porosimetry has been used to determine the pore size distribution of PolyHIPE materials;[8] however, it should be pointed out that for PolyHIPEs this technique provides information only about the size of the interconnecting windows and not the void size. In Table 5, values of the average window diameters ($\langle \Delta \rangle$) and pore volumes (V_p) determined by mercury intrusion porosimetry, for PolyHIPEs characterized by different in-

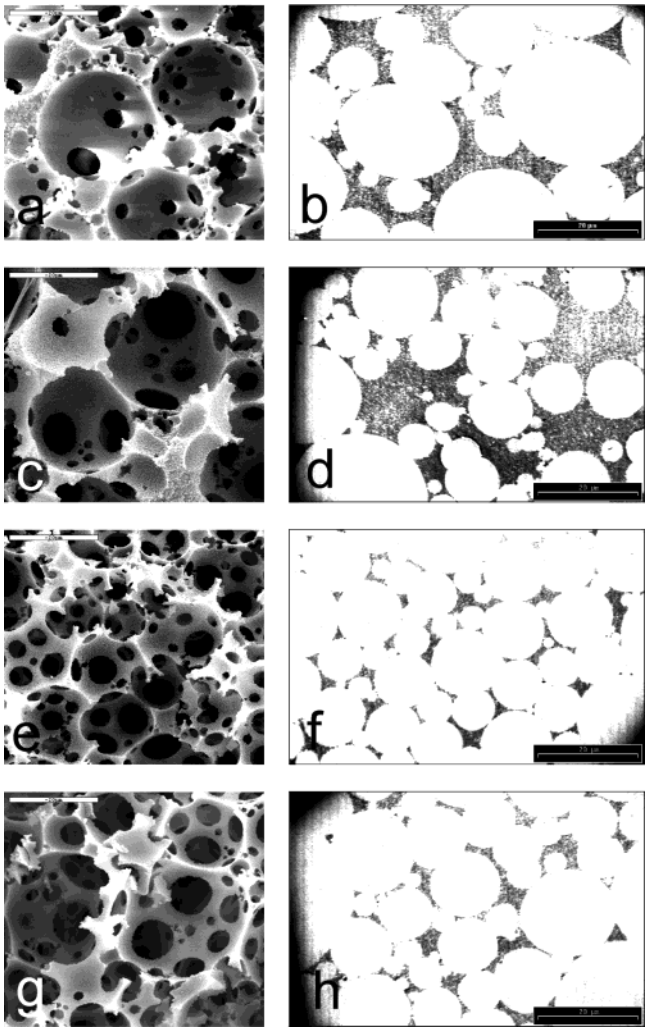

Figure 8. SEMs (left column) and TEMs (right column) of PolyHIPE solid foams characterized by increasing pore volume: (a and b) X80PV75(1CB)S80; (c and d) X80PV85(1CB)-S80; (e and f) X80PV90(1CB)S80; (g and h) X80PV92(1CB)S80. Scale bar = 20 μm.

Table 5. Characterization of PolyHIPE Solid Foams with Different Pore Volumes

sample[a]	$\langle D \rangle$ (μm)[b]	$\langle d \rangle$ (μm)[c]	$\langle d \rangle / \langle D \rangle$	$\langle \Delta \rangle$ (μm)[d]	V_p (cm^3/g)[e]
X80PV75(1CB)S80	8.2	2.9	0.34	4.0	6.0
X80PV85(1CB)S80	7.3	2.9	0.40	6.4	11.2
X80PV90(1CB)S80	9.8	4.5	0.46	8.1	12.4
X80PV92(1CB)S80	10.5	5.3	0.51		

[a] See Experimental Section for sample coding system. [b] Average void diameter determined by TEM. [c] Average window diameter determined by TEM. [d] Relative average window diameter determined by intrusion Hg porosimetry. [e] Pore volumes obtained by Hg porosimetry.

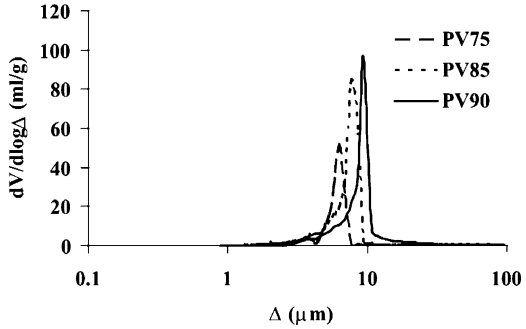

Figure 9. Mercury intrusion porosimetry window size distributions of DVB 80% PolyHIPE solid foams prepared using CB as a porogen, SPAN 80 as surfactant and characterized by increasing pore volume: PV75 (dashed line); PV85 (broken line); PV90 (solid line).

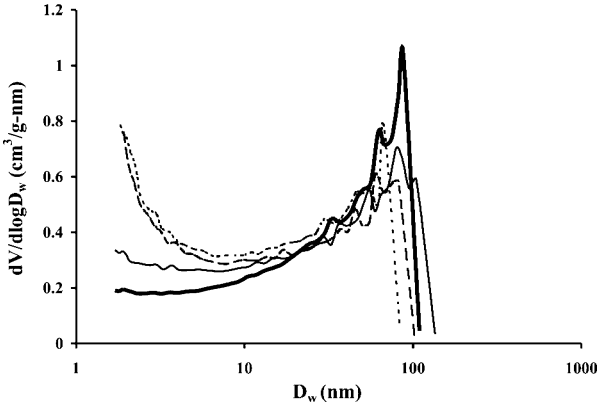

Figure 10. N_2 BJH adsorption pore size distribution of PolyHIPE solid foams prepared by using SPAN 80 as a surfactant and CB as a porogen and characterized by increasing pore volume: PV92 (heavy line); PV90 (solid line); PV85 (dotted line); PV75 (dashed line).

ternal phase volume ratios, are shown. The corresponding window size distribution plots are shown in Figure 9. It can be seen that values of $\langle\Delta\rangle$ deviate from $\langle d\rangle$ values determined by TEM, and the deviation increases as pore volume increases. This is because $\langle\Delta\rangle$ is subject to a systematic error. The function used to calculate $\langle\Delta\rangle$, dV/d(log Δ), is a volume distribution function, with the result that $\langle\Delta\rangle$ differs from the "real" window diameters determined by TEM and that this difference increases with pore volume. Therefore, it should be appreciated that there are errors associated with values of $\langle\Delta\rangle$ particularly at high pore volumes and this should be borne in mind when interpreting results.

Furthermore, Hg results must be examined with caution in another respect. Specimens are subject to high pressures, which may compress them and distort the data to give erroneous values for window sizes. This effect, if present, would be more pronounced for high PV solid foams because they are characterized by thinner walls. Precautions were taken in order to avoid this (see Experimental Section). For this reason mercury intrusion porosimetry results were judged unreliable in the case of X80PV92(1CB)S80. Data relative to pore volume (Table 5) seem to indicate that the sample with PV 90 suffered some compression. In fact the ratio between volumes of dispersed phase corresponding to PV 85 and 75 and that for intrusion volumes, coincide ($\approx$1.9). On the contrary, the same comparison between PV 90 and 85 reveals that the experimental ratio deduced from intrusion data (1.1) is lower than the theoretical one (1.6). Clearly, this compression is due to the thinner walls of the PV90 solid foam as compared to PV85. It can be concluded that TEM data are undoubtedly more reliable and provide a wider range of information ($\langle D\rangle$, $\langle d\rangle$, and $\langle d\rangle/\langle D\rangle$) than mercury intrusion porosimetry when characterizing PolyHIPEs.

N_2 adsorption shows that the first two solid foams characterized by a lower PV (75 and 85%) have similar surface areas, pore volumes and average pore diameters in the range between 1.7 and 200 nm (Table 2, entries 6 and 7). About 10% of the surface area is due to the presence of micropores (diameter < 2 nm). The surface areas of solid foams with PV > 85 (Table 2, entries 2 and 8) tend to decrease proportionally with PV. As the composition of the organic phase in the precursor emulsions is exactly the same for X80PVN(1CB)S80 type solid foams, the physical variables responsible for the transition described above must be related to PV. The variables on which the volume of the dispersed phase exerts an influence are the droplet dimensions, degree of packing (Figure 8 and Table 5), and presumably the surfactant interfacial excess. BJH adsorption dV/d(log D_w) pore size distributions, where D_w is the diameter of pores within the walls (Figure 10), are quite broad spanning over 2 orders of magnitude and show that the proportion of mesopores increases progressively with decreasing PV. Accordingly, the surface areas increase in the same fashion and the average pore diameter decreases (Table 2).

The surfactant molecules present in the organic phase are distributed between the interface and reverse micelles. As the aqueous/oil phase ratio increases, the water−oil interface area increases and some of the surfactant molecules present in the bulk of the organic phase will be adsorbed at the interface to cover the newly created interfacial area. As a consequence, the number of reverse micelles decreases with increasing water content, and as the water fraction approaches 1, no reverse micelles are present in the continuous phase. Also, the absolute amount of surfactant present in the dispersed phase in the form of submicelles will increase with the PV. Opawale et al.[38] showed that the effect of SPAN 80 bulk concentration above cmc on the interfacial tension at the mineral oil/water interface seemed to indicate the occurrence of multilayer adsorption/association. Their study also indicated that excess surfactant may be advantageous for emulsion stability, as the interfacial elasticity and hence film strength increases with surfactant concentration. This effect has also been observed in different systems, for instance asphaltene dissolved in heptol.[39]

The mechanism through which PV affects the porous structure of the solid foams may be related to the state of the surfactant at the O/W interface. The concentration of SPAN 80 in the oil phase is close to 0.5 M (20 wt % based on monomer plus porogen used). Because of the presence of a high level of CB (a relatively polar molecule, see Table 3), the polarity of the organic medium is expected to be high and as a consequence SPAN 80 cμc might be of the same order of magnitude as the actual concentration of SPAN 80 in the organic phase. The similarity of surface area and porosity data between X80PV75(1CB)S80 and X80PV85(1CB)S80 might indicate that the surfactant concentration is, at the temperature of polymerization (60 °C), at or above cμc In such a situation the interface is completely coated by a mono/multilayer film of surfactant and the interfacial tension is at its minimum. When PV is increased

to 90 and 92%, it can be envisaged that because of the larger surface over which the surfactant has to spread and taking into account that the amount of surfactant, dissolved in the aqueous phase, increases with PV, the surfactant concentration in the oil phase at 60 °C is below cμc In this situation the interface is not completely saturated with surfactant molecules and the interfacial tension is above its minimum value.

We tried to measure the interfacial tension between the preequilibrated aqueous and organic phases by the spinning drop method[40] to provide experimental support to the hypothesis of a change of interfacial excess with PV. It turned out that the densities of the aqueous and organic phases were very similar, differing by less than 1%, which prevented the successful application of this technique.

The redistribution of surfactant molecules which takes place with the increase of PV affects the concentration and size of the W/O microemulsion droplets in the continuous phase. This will in turn affect the porosity of the solid foams. In this case the decrease of surface area should be monotonic, while experimentally we found that for PV 75 and 85 the values are similar (Table 2, entries 6 and 7) and also the values obtained at higher PV (from 470 to 236 $m^2\ g^{-1}$ from PV 85 to 92, respectively) are well beyond the surface areas possible through microemulsion templating. Moreover, the pore volume values provided by N_2 porosimetry are basically constant for the variable PV solid foams (Table 2). This seems to imply that there is not a significant contribution from pores ensuing from microemulsion templating because, otherwise, the pore volume should change following a variation of PV.

Therefore, the correlation between N_2 adsorption data and PV must rely on a different kind of phenomenon. To obtain more clues, we investigated the role of monomer-to-porogen ratio on the pore microstructure of PolyHIPEs as evidenced by N_2 sorption data. In Table 2, entry 9, porosity data for a PolyHIPE solid foam obtained with a monomer to porogen (CB) ratio of 1:0.5 is reported. Surprisingly, the surface area of X80PV90-(0.5CB)S80 is, within experimental error, the same as X80PV90(1CB)S80 (Table 2, entry 2). When the monomer-to-porogen ratio is 1:1 the surface area is expected to be higher than when this ratio is 1:0.5, because the growing polymeric network is better solvated and phase separation occurs at later stages of polymerization. When phase separation occurs, most of the monomer has already reacted and the fine porous structure (i.e., in the mesopore, 2−50 nm, and micropore, <2 nm, regions) is preserved. On the contrary when the porogen induces polymer network phase separation at much lower monomer conversion, macroporous resins characterized by lower surface areas and broad pore size distributions are obtained.[41] The experimental evidence reported concerning the effect of PV and monomer-to-porogen ratio on DVB 80% PolyHIPE microstructure shows that the actual composition of the organic medium in the corresponding emulsions has changed from the initially prepared organic phase solution. Nitrogen adsorption data (Table 2) show that the surface areas are relatively low despite the good quality of the porogenic solvents employed and the pore size distribution is broad (Figures 4 and 10), which indicates that the organic medium does not have optimal solvating properties toward the polymeric matrix (Table 4 and Figure 7d). When CB[36] is used as a porogen in the bulk polymerization of DVB 80%, a resin with a surface area as high as 850 m^2/g and a narrow pore size distribution can be produced. It is reasonable to assume that the effect exerted by variation of PV and monomer/porogen ratio on solid foam microstructure has a common origin.

In Table 2 are reported nitrogen adsorption results for solid foams containing CEB as a porogen, at a monomer-to-porogen ratio of 1:0.5 and 1:1 vol:vol (entries 10 and 4, respectively) and at two different nominal PVs, 75 and 90% (entries 11 and 4 respectively). The comparison of surface area data between these solid foams with the corresponding ones prepared by employing CB as a porogen, reveals a completely different behavior. When CEB is used, the surface areas of the solid foams characterized by a constant PV (90%) but at different monomer-to-porogen ratios, 1:1 and 1:0.5 (X80PV90(1CEB)S80 and X80PV90(0.5CEB)S80) are approximately in a 1:0.35 ratio as opposed to the approximately 1:1 ratio exhibited by the same kind of solid foams prepared using CB. At constant monomer-to-porogen ratio but at two different PVs, 75 and 90% (X80PV75(1CEB)S80 and X80PV90(1CEB)S80), the relative surface areas are close to each other, the surface area of the latter being about 18% higher. The influence of the PV on surface area is the opposite to that occurring in the series X80PVN(1CB)S80. These results allow the inference that it is the nature of the porogen which is responsible for the dependence of solid foam microstructure on PV and on monomer-to-porogen ratio. Previously,[9] we have provided some evidence that CEB has the tendency to be coadsorbed at the interface with the primary surfactant SPAN 80, increasing the interface excess and reducing the interfacial tension. This effect was exploited in the preparation of a PolyHIPE solid foam X80PV90(0.5CB + 0.5CEB)S80, possessing a high surface area, 570 m^2/g^{-1}, from an emulsion containing a porogenic mixture of CB and CEB in a 1:1 vol:vol ratio.

The set of results detailed so far is consistent with the suggestion that the phenomenon mainly responsible for the dependence of solid foam microstructure on PV and on monomer-to-porogen ratio is Ostwald ripening. This is the process by which large droplets grow at the expense of smaller ones due to the difference in their chemical potential. In Ostwald ripening the growth occurs by diffusion of the dispersed through the continuous phase. The kinetics of Ostwald ripening is most often described in terms of the LSW theory:[42]

$$\omega = \frac{\mathrm{d}a_c^{\,3}}{\mathrm{d}t} = \frac{8c(\infty)\gamma V_m D}{9RT} f(\phi) \qquad (4)$$

where a_c is the critical radius of a drop which at a given time is neither growing nor decreasing in size, $c(\infty)$ is the solubility of the dispersed phase in an infinite sized drop, i.e., at a planar interface, γ is the interfacial tension, V_m is the molar volume of the dispersed phase, D is the diffusion coefficient of the dispersed phase in the continuous phase, $f(\phi)$ reflects the dependence of the rate of ripening, ω, on the dispersed phase volume fraction, ϕ, and R is the gas constant.

Analysis of eq 4 is of help in the interpretation of the results obtained from the series of PolyHIPEs presented so far. For instance, as stated above, it is expected that the surface area of X80PV90(1CB)S80 would be higher than that of X80PV90(0.5CB)S80, because a higher level of porogen is more effective in solvating the growing

polymeric network during polymerization. The results obtained (Table 2, entries 2 and 9) contradict this expectation; the surface areas are the same within experimental error. A reasonable explanation relies on the correlation with the term $c(\infty)$ in eq 4. A higher concentration of CB in the organic phase should favor the dissolution of a higher amount of water, because the affinity of the continuous phase toward the dispersed phase should increase. As shown in Table 3, CB as a solvent combines a relatively high polarity (δ_p) with some hydrogen bonding capability (δ_h). For this reason the value of $c(\infty)$ should be higher for the emulsion characterized by a 1:1 than a 1:0.5 monomer-to-porogen ratio. Hence the rate of ripening should be faster in the former case.[42] Because of water diffusion, there is a balancing effect between the amount of porogen which favors the creation of a solid foam with a high surface area and the amount of water dissolved in the organic phase which tends to turn the porogenic medium into a poor one for the polymer. As a result of these opposing effects, X80PV90(1CB)S80 and X80PV90(0.5CB)S80 have comparable surface areas.

The rate of ripening depends also on the interfacial tension, γ. The presence of a surfactant has itself a stabilizing effect toward Ostwald ripening because of the reduction of interfacial tension and the creation of a barrier which opposes diffusion. If a cosurfactant capable of inserting among the primary surfactant molecules adsorbed at the interface is present, an additional stabilizing force results. This is the case of the emulsion containing the mixture of CB and CEB.[9] The additional lowering of interfacial tension ensuing from the coadsorption of CEB molecules at the interface, slows the diffusion of water through the continuous phase and a PolyHIPE with a much higher surface area is obtained, X80PV90(0.5CB+0.5CEB)S80.[9]

The same kind of phenomenon is probably occurring when the PV is changed in the series X80PVN(1CB)-S80. At low PV (75 and 85%) and at 60 °C, the surfactant interface excess might be higher than at 90 and 92% PV, and as a consequence, the interfacial tension could be lower and the interfacial film less penetrable by water molecules.

The tendency of CEB molecules to be adsorbed at the interface also allows us to explain the surface areas of solid foams prepared from emulsions containing CEB as a porogen. When the monomer-to-porogen ratio is 1:0.5, the surface area is well below that of the solid foam prepared with a 1:1 ratio. This is probably due to the depletion of CEB molecules from the bulk of the continuous phase upon adsorption at the interface. This depletion is likely to be proportionately greater in the 1:0.5 monomer:porogen ratio HIPE than for the 1:1 one. This would explain why the effect on the solid foam porosity is greater for X80PV90(0.5CEB)S80 than for X80PV90(1CEB)S80. The effect of PV on porosity is much less pronounced for solid foams prepared with CEB than that exhibited by solid foams with CB as a porogen. The surface area corresponding to PV90 is higher than 75. This result allows us to rule out the hypothesis that variation in surface areas in the series X80PVN(1CB)S80 was due to variation in the surfactant interface excess, because this should also be true for solid foams of the X80PVN(1CEB)S80 type. This difference may again be explained by the tendency of CEB molecules to be adsorbed at the interface: proportionately, the amount of CEB molecules adsorbed should be less for the PV75 compared to the PV90 solid foam, because the interfacial area is lower. This will leave a higher concentration of CEB in the bulk of the continuous phase of the PV75 solid foam. The gradient in polarity across the interface will then be more pronounced allowing the diffusion of more water with the result that the final surface area of X80PV75(1CEB)-S80 will be lower than that of X80PV90(1CEB)S80.

Variation in porosity data observed in solid foams of the X80PVN(1CB)S80 type may be a consequence of the influence of PV on $f(\phi)$. Interdroplet diffusional interactions will affect the dynamics of Ostwald ripening to an extent which is dependent on PV. As the average distance between the droplets of the dispersed phase decreases, the diffusion domains originating from different droplets tend to overlap. In these zones, the concentration of water rises above the rest of the continuous phase, worsening substantially the quality of the reaction medium. The solubility parameter of water (Table 3) is much higher than those of the components of the continuous phase of the emulsion, so it may be envisaged that the differences in surface areas we have measured can be traced back to small differences in the concentration of water dissolved in the continuous phase. The void distributions of solid foams characterized by increasing PV as evidenced by TEM micrographs (Figure 8) correlate well with the surface area results (Table 2). We have already pointed out how the increase in PV involves a more compact arrangement in space of the droplets of the dispersed phase, decreasing the average distance among them. The dependence of Ostwald ripening on $f(\phi)$ may also explain the anomaly represented by the increase in surface area when passing from PV 75 to 85 (Table 2). TEM (Figure 8d) clearly shows that, for the PV 85 solid foam, voids tend to be grouped together leaving relatively large areas free of voids. The PV75 solid foam presents a more homogeneous void distribution. It may be envisaged that outside the clusters in PV85 there is rather limited superimposition of the diffusion spheres while inside they overlap to a much larger extent. The outcome in terms of porosity is a solid foam which propably exhibits zones of different porosity and with an overall surface area slightly higher than X80PV75-(1CB)S80.

Conclusions

The influence of oil-phase soluble porogens on the structure of poly(divinylbenzene) PolyHIPE materials prepared with SPAN 80 as surfactant has been investigated. The discussion presented above shows that a porogenic solvent may play multiple roles in determining the final morphology of a PolyHIPE solid foam. These are as follows:

(1) The compatibility of the porogenic solvent with poly(DVB 80%) (i.e., possessing a solubility parameter similar to that of poly(DVB 80%)). The higher the compatibility, the higher the solid foam surface area.

(2) The surface activity of the porogenic solvent used. It is well-known that shorter chain and polar molecules tend to penetrate between the chains of a surfactant monolayer to a larger degree, creating a wedge effect on the oil side of the monolayer and increasing the spontaneous curvature.[28] As argued above the lowering of interfacial tension and possibly the creation of a more coherent film could reduce the rate of diffusion of the dispersed through the continuous phase (Ostwald ripen-

ing), thus preserving the swelling property of the porogen toward the polymer.

(3) The polarity of the porogen. Arguably, the higher the polarity of the solvent and the greater its ability to form hydrogen bonds with water, the higher will be its ability to incorporate increasingly larger quantities of water. In other words, the weight of the term $c(\infty)$ in eq 4 becomes increasingly more pronounced. In a similar fashion the amount of porogen which partitions with the aqueous phase should increase with porogen polarity. This property may also affect the surfactant $c\mu c$ and consequently the degree of coverage of the oil/water interface.

It should be stressed that in this article, for the first time, we have described the physical phenomena (Ostwald ripening and porogen adsorption at the interface) that determine the morphology and porosity of PolyHIPEs. This is important because the identification and understanding of these phenomena allow measures to be taken to control or suppress them. The materials described here differ in three ways from those reported by Sherrington et al.:[8] (i) The surface areas are significantly higher (e.g., 570 vs 350 $m^2\ g^{-1}$). (ii) The mechanical properties (qualitative assessment) are much better—one of the PolyHIPE materials described previously (X80PV90(1T)) was reproduced and found to crumble very easily on handling, whereas the materials prepared here are easily manipulated without any noticeable damage. This may be due to the significantly higher quantity of SPAN 80 (33% (w/w)) used by Sherrington et al. to prepare PolyHIPEs. (iii) Many of the solid foams have smaller average void diameters, which may be an advantage for applications such as solid-phase synthesis and analytical separations.

The large differences between surface area values and porosity data of the porous DVB 80% resins reported in Table 2 and the corresponding PolyHIPE solid foams obtained from emulsions containing CB, C_2B, CEB, and T as porogens seem to indicate that diffusion of the dispersed through the continuous phase and possibly partitioning of the porogen between the two phases are the dominant processes in determining the microstructure of these solid foams. As to what extent these phenomena occur, the nature of the surfactant should play a fundamental role. SPAN 80 as a surfactant presents some drawbacks: the oleic tail is in the cis configuration and this prevents to some extent an efficient packing of surfactant molecules in the interfacial film.[7,43] In the following article, we demonstrate that a three-component surfactant system that produces a much more compact interfacial film, which inhibits Ostwald ripening, does indeed give rise to analogous PolyHIPEs with significantly different morphologies and higher surface areas.

Acknowledgment. The authors thank the EPSRC for funding this research (GR/M02194).

References and Notes

(1) Lissant, K. J., Ed.; *Emulsions and Emulsion Technology Part 1*; Marcel Dekker Inc.: New York, 1974.
(2) Ruckenstein, E. *Adv. Polym. Sci.* **1997**, *127*, 1−58.
(3) Bartl, H.; von Bonin, W. *Makromol. Chem.* **1962**, *57*, 74−95. Barby, D.; Haq, Z. Eur. Pat. Appl., 60138, 1982. Cameron, N. R.; Sherrington, D. C. *Adv. Polym. Sci.* **1996**, *126*, 163-214. Cameron, N. R. *J. Chromatogr. Libr.* **2003**, *67*, 255−276.
(4) Williams, J. M.; Wrobleski, D. A. *Langmuir* **1988**, *4*, 656−662.
(5) Williams, J. M. *Langmuir* **1988**, *4*, 44−49. Williams, J. M. *Langmuir* **1991**, *7*, 1370−1377.
(6) Williams, J. M.; Gray, A. J.; Wilkerson, M. H. *Langmuir* **1990**, *6*, 437−444.
(7) Barbetta, A.; Cameron, N. R.; Cooper, S. J. *Chem. Commun.* **2000**, 221−222.
(8) Hainey, P.; Huxham, I. M.; Rowatt, B.; Sherrington, D. C.; Tetley, L. *Macromolecules* **1991**, *24*, 117−121.
(9) Cameron, N. R.; Barbetta, A. *J. Mater. Chem.* **2000**, *10*, 2466−2472.
(10) Sing, K. S. W.; Everett, D. H.; Haul, R. A. W.; Moscou, L.; Pierotti, R. A.; Rouquerol, J.; Siemieniewska, T. *Pure Appl. Chem.* **1985**, *57*, 603−619.
(11) Sherrington, D. C. *Chem. Commun.* **1998**, 2275.
(12) Brunauer, S.; Emmett, P. H.; Teller, E. *J. Am. Chem. Soc.* **1938**, *60*, 309.
(13) *Porosity and pore size distribution of materials*; BS 7591, Part 2, British Standards Institute: London, 1992.
(14) Busby, W.; Cameron, N. R.; Jahoda, C. A. B. *Biomacromolecules* **2001**, *2*, 154−164. Busby, W.; Cameron, N. R.; Jahoda, C. A. B. *Polym. Int.* **2002**, *51*, 871−881.
(15) Peters, E. C.; Svec, F.; Frechet, J. M. J. *Adv. Mater.* **1999**, *11*, 1169−1181.
(16) Gregory, D. P.; Sharples, M.; Tucker, I. M. *Eur. Pat. Appl.* **1989**, 299762.
(17) Cameron, N. R.; Sherrington, D. C.; Albiston, L.; Gregory, D. P. *Colloid Polym. Sci.* **1996**, *274*, 592−595.
(18) Rohr, T.; Knaus, S.; Gruber, H.; Sherrington, D. C. *Macromolecules* **2002**, *35*, 97−105.
(19) Nyhus, A. K.; Hagen, S.; Berge, A. *J. Polym. Sci., Part A: Polym. Chem.* **1999**, *37*, 3973−3990.
(20) Rabelo, D.; Coutinho, F. M. B. *Polym. Bull. (Berlin)* **1994**, *33*, 479−486.
(21) Rabelo, D.; Coutinho, F. M. B. *Polym. Bull. (Berlin)* **1994**, *33*, 487−491. Rabelo, D.; Coutinho, F. M. B. *Polym. Bull. (Berlin)* **1994**, *33*, 493−496.
(22) Barton, A. F. M., Ed. *Handbook of Solubility Parameters and Other Cohesion Parameters*, 2nd ed.; CRC Press: Boca Raton, FL, 1991.
(23) Brandrup, J.; Immergut, E. H.; Grulke, E. A. *Polymer Handbook*, 4th ed.; Wiley: New York, 1999.
(24) van Krevelen, D. In *Properties of Polymers*, 3rd ed.; Elsevier: Amsterdam, 1991; Chapter 7, p 189.
(25) Rabelo, D.; Coutinho, F. M. B. *Eur. Polym. J.* **1994**, *30*, 675−682.
(26) Poinescu, I. C.; Vlad, C.-D. *Eur. Polym. J.* **1997**, *33*, 1515.
(27) Boyde, A. In *Scanning Electron Microscopy*; Wells, O. C., Ed.; McGraw-Hill: New York, 1974.
(28) Kabalnov, A. S.; Makarov, K. N.; Pertsov, A. V.; Shchukin, E. D. *J. Colloid Interface Sci.* **1990**, *138*, 98−104.
(29) Ravey, J. C.; Stebe, M. J. *Prog. Colloid Polym. Sci.* **1990**, *82*, 218−228. Pons, R.; Erra, P.; Solans, C.; Ravey, J. C.; Stebe, M. J. *J. Phys. Chem.* **1993**, *97*, 12320−12324. Pons, R.; Ravey, J. C.; Sauvage, S.; Stebe, M. J.; Erra, P.; Solans, C. *Colloids Surf., A: Physicochem. Eng. Aspects* **1993**, *76*, 171−177. Ravey, J. C.; Stebe, M. J.; Sauvage, S. *Colloids Surf., A: Physicochem. Eng. Aspects* **1994**, *91*, 237−257.
(30) Menger, F. M.; Tsuno, T.; Hammond, G. S. *J. Am. Chem. Soc.* **1990**, *112*, 1263−1264. Stoffer, J. O.; Bone, T. *J. Dispersion Sci. Technol.* **1980**, *1*, 393−412. Sasthav, M.; Raj, W. R. P.; Cheung, H. M. *J. Colloid Interface Sci.* **1992**, *152*, 376−385.
(31) Haque, E.; Qutubuddin, S. *J. Polym. Sci., Part C: Polym. Lett.* **1988**, *26*, 429−432. Sasthav, M.; Cheung, H. M. *Langmuir* **1991**, *7*, 1378−1382.
(32) Guo, J. S.; El-Aasser, M. S.; Vanderhoff, J. W. *J. Polym. Sci., Part A: Polym. Chem.* **1989**, *27*, 691−710. Jayakrishnan, A.; Shah, D. O. *J. Polym. Sci., Polym. Lett. Ed.* **1984**, *22*, 31−38. Landau, F. In *Encyclopedia of Polymer Science and Engineering*; Mark, H. F., Bilakes, N. M., Overberger, C. G., Menges, F., Eds.; Wiley: New York, 1987; Vol. 9, p 718.
(33) Zhu, X. X.; Banana, K.; Liu, H. Y.; Krause, M.; Yang, M. *Macromolecules* **1999**, *32*, 277−281.
(34) Menger, F. M.; Tsuno, T. *J. Am. Chem. Soc.* **1990**, *112*, 6723−6724.
(35) Binks, B. P.; Fletcher, P. D. I.; Horsup, D. I. *Colloids Surf.* **1991**, *61*, 291−315.
(36) Santora, B. P.; Gagne, M. R.; Moloy, K. G.; Radu, N. S. *Macromolecules* **2001**, *34*, 658−661.
(37) Webb, P.; Orr, C. *Analytical Methods in Fine Particle Technology*; Micromeritics Instrument Corp.: Norcross, GA, 1997.

(38) Smith, D. M.; Hua, D. W.; Earl, W. L. *MRS Bull.* **1994**, *19*, 44−48. Whang, K.; Thomas, C. H.; Healy, K. E.; Nuber, G. *Polymer* **1995**, *36*, 837−842.
(39) Aronson, M. P.; Petko, M. F. *J. Colloid Interface Sci.* **1993**, *159*, 134−149.
(40) Opawale, F. O.; Burgess, D. J. *J. Colloid Interface Sci.* **1998**, *197*, 142−150.
(41) Krawczyk, M. A.; Wasan, D. T.; Shetty, C. *Ind. Eng. Chem. Res.* **1991**, *30*, 367−375.
(42) Vonnegut, B. *Rev. Sci. Instrum.* **1942**, *13*, 6−9.
(43) Guyot, A. In *Syntheses and Separations Using Functional Polymers*; Sherrington, D. C., Hodge, P., Eds.; Wiley: Chichester, U.K. 1988; Chapter 1.
(44) Lifshitz, I. M.; Slezov, V. V. *Phys. Chem. Solids* **1961**, *19*, 35. Wagner, C. *Z. Elektrochem. Angew. Phys. Chem.* **1961**, *65*, 581−591. Kabalnov, A. S.; Pertsov, A. V.; Shchukin, E. D. *J. Colloid Interface Sci.* **1987**, *118*, 590−597.
(45) Mitchell, D. J.; Ninham, B. W. *J. Chem. Soc., Faraday Trans. 2: Mol. Chem. Phys.* **1981**, *77*, 601−629. Aveyard, R.; Binks, B. P.; Fletcher, P. D. I.; MacNab, J. R. *Langmuir* **1995**, *11*, 2515−2524. Rosen, M. J. In *Surfactants and Interfacial Phenomena*, 2nd ed.; Wiley: New York, 1989; 6.

MA0359436